Theoretical and experimental study of a 30 nm metallic slot array

Qing Tan,* Armando Cosentino, Matthieu Roussey, and Hans Peter Herzig

Ecole Polytechnique Fédérale de Lausanne (EPFL) Optics & Photonics Technology Laboratory
Breguet 2, 2000, Neuchâtel Switzerland
*Corresponding author: qing.tan@epfl.ch

We present the simulation, fabrication, and characterization of a metallic slot grating on a silicon waveguide (30 nm slot width for a period of 500 nm). According to the simulation, the experimental measured spectrum of the structure exhibits a dip in the near-infrared region. Moreover, the finite-difference time-domain simulation shows that this device can be used as a sensor, due to its high sensitivity to the refractive index variation of the medium above and inside the cavity ($\eta = \Delta\lambda/\Delta n = 750$ nm/refractive index unit).   © 2011 Optical Society of America

OCIS codes: 310.6628, 310.6805, 220.4241, 130.6010.

1. INTRODUCTION

Optical sensors [1] based on refractive index detection are attractive due to their high sensitivity and the label-free method they provide. The two most commonly used techniques are optical fiber based sensors [2–4], which can achieve a resolution down to 10^{-5} refractive index unit (RIU), and surface plasmon resonance technique based sensors [5–8], with an obtained resolution as high as 10^{-8} RIU [9]. Attempts for miniaturizing these sensors have been done using photonic crystal cavities [10], but decreasing the size of the sensor means decreasing its sensitivity proportionally to the interaction strength between light and analyte. It is evident that a compromise between the size of the sensor and the sensitivity has to be found. Metallic nanostructure devices [11,12] are promising candidates to obtain a high enhancement and confinement of the electromagnetic field in a small volume. Recently, Brolo *et al.* [13] explored a sensor based on the enhanced light transmission through hole arrays in gold films. Veronis and Fan [14] and Dionne *et al.* [15] have shown how a plasmonic mode can be supported and confined in a subwavelength slot of a few tens of nanometers width. Experimental demonstrations are still rare, and one attempt has been done by Chen *et al.* in 2006 [16]. In that paper they studied the properties of a 150 nm slot silicon waveguide covered by gold. We propose here an application of such a kind of device to sensing. Its integration with dielectric structures takes the advantage of a small analyte volume in the slot region and shows good compatibility with other photonic devices, such as photonic crystals. The device design and property simulation, fabrication process, and experimental measurements will be sequentially illustrated in the following sections.

2. DESIGN AND SIMULATION

The schematic view of the designed device is shown in Fig. 1. It consists of a dielectric slab waveguide and a thin film gold (Au) cavity. The waveguide is composed of a 100 nm silicon dioxide (SiO_2) layer and a 220 nm silicon (Si) layer, deposited on a Si/SiO_2 substrate. The cavity is a periodic slot array ex-

tended in the x direction. The geometric parameters are slot width (w), gold thickness (h), cavity length (l), and periodicity (p). In this device, light propagates through the Si slab waveguide and is coupled to the Au cavity at the surface of the waveguide via an evanescent wave.

The three-dimensional (3D) finite-difference time-domain (FDTD) method is used to model the optical property and response of the device. In the model, periodic boundary condition is used to mimic the infinity of the structure in x direction, and perfectly matched layers are used in the two other directions (y and z). The illumination is the optical mode supported by the waveguide ($SiO_2/Si/SiO_2$). An adaptive mesh is considered in this model: the step size is 2 nm in the Au cavity area and about 20 nm in the other region. Note that the dispersion property of Au is taken into account thanks to the Drude model [Eq. (1)]:

$$\varepsilon_{\mathrm{Au}} = 1.0 - \frac{\omega_p^2}{\omega^2 - i\omega\gamma}, \tag{1}$$

where the bulk plasma frequency is $\omega_p = 1.2 \times 10^{16}\,\mathrm{s}^{-1}$ and the damping rate is $\gamma = 1.25 \times 10^{14}\,\mathrm{s}^{-1}$. The chosen values allow fitting in good agreement with the real values of the material in the wavelength range of interest. The dielectric constants for Si and SiO_2 are set to be $\varepsilon_{\mathrm{Si}} = 11.97$ ($n_{\mathrm{Si}} = 3.46$) and $\varepsilon_{\mathrm{SiO_2}} = 2.074$ ($n_{\mathrm{SiO_2}} = 1.44$), respectively. The cavity parameters are $p = 500$ nm, $l = 800$ nm, $h = 20$ nm, and $w = 20$ nm.

The transmission spectrum of the structure (including the waveguide and the substrate) is given in Fig. 2(a) for transverse magnetic polarized light. One can observe three transmission dips, A, B, and C, corresponding to the resonances of the structure. The normalized electric field intensity $|E|^2$ distribution and the phase profile φ along the light propagation direction ($+z$) in the middle of the slot are shown in Fig. 2(b) for the three resonances A, B, and C. The intensity $|E|^2$ profiles in the $+z$ direction show that the electric field is highly confined in the air-slot region. Even though light is confined in the air slot over the whole spectrum due to the finite width (x direction) of the slot, the field localization is further enhanced
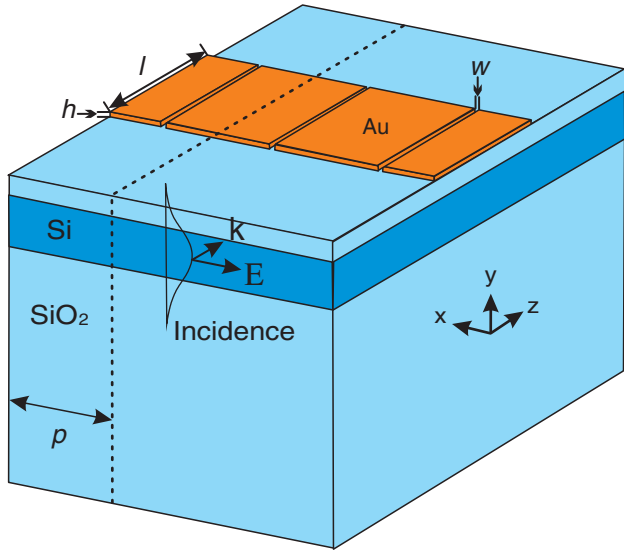
Fig. 1.   (Color online) Schematic view of the studied device with periodic extension in the x direction. The cavity parameters are slot width (w), gold thickness (h), cavity length (l), and periodicity (p). The Si waveguide is first fixed to be 100 and 220 nm thick for the top SiO$_2$ layer and the Si layer, respectively.

at the three transmission dips. This localization is due to the Fabry–Perot (FP) behavior of the cavity, which improves the evanescent wave coupling efficiency to the slots. The phase profiles in Fig. 2 show that the phase difference between the forward and backward waves in the cavity is equal to π, 2π, and 3π for dips A, B, and C, respectively. It corresponds to the resonance condition of a classical FP: $\varphi = q\pi$, where q is an integer. Dips A, B, and C correspond to the three first modes of the FP. The intensity distribution in the air slot has one, two, and three zeros, respectively. In the following, only the second mode (B) will be considered. Indeed, two reasons make this dip interesting for the sensing application. First, dip A is too large and dip C is too shallow to perform significant measurements. Second, the field localization mainly centered in the middle of the slot will confer to the structure a more stable response, even with fabrication imperfections.

Veronis and Fan [14] have shown that the field confinement of the supported mode inside the slot depends drastically on the geometry. Furthermore, the FP-like resonance, which plays a major role in the dip position determination with regard to the mode effective refractive index, enhances the field localization in the cavity. Therefore, the λ_d position of dip B is sensitive to the cavity geometry. An analysis is made to determine the λ_d variation with the geometric parameters (a) slot width w, (b) gold thickness h, and (c) cavity length l. The results are reported in Fig. 3. Each solid curve is mathematically fit from discrete calculated points. In Fig. 3(c), λ_d is almost linearly related to the length of the cavity in the range of interest, which is in accordance with the phase-matching condition of the FP resonance. Graphs (a) and (b) show that the field localization of the supported mode in the air slot is highly sensitive to the slot size, slot width (w) and Au thickness (h) in our case. Verified by Veronis and Fan [14], the smaller air slot has a stronger field intensity in the air region and more energy loss in Au. As a result, λ_d exponentially blueshifts by the increase of w or h. When the air slot is enlarged enough, the slot
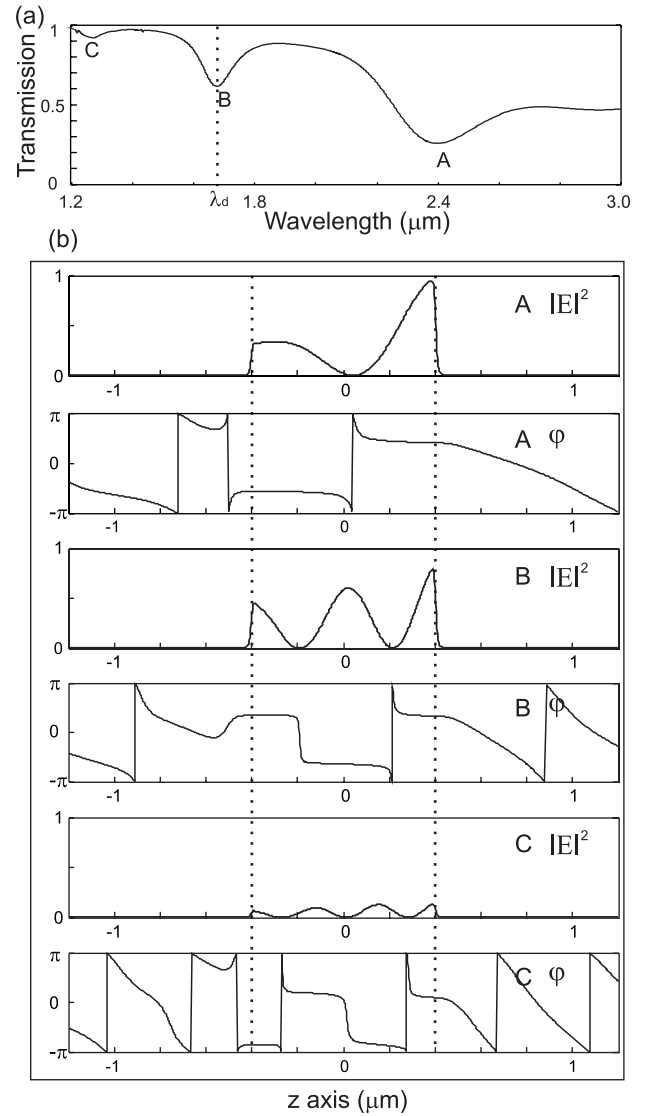

Fig. 2.   Simulated optical properties for a device with parameters $p = 500$ nm, $l = 800$ nm, $h = 20$ nm, and $w = 20$ nm. (a) Normalized transmission spectrum and (b) normalized $|E|^2$ distribution and phase φ profile along the central line of the air slot for different wavelengths shown as points A, B, and C in (a), respectively.

hardly confines light and the transmission dip is too weak to be distinguished.

Besides the slot geometry, the refractive index of the material filling the slot is another parameter that has an effect on the light confinement in the slot. The analyte will be placed above and in the slot cavity. The effective wavelength of light is shortened with a larger material index. By measuring λ_d, one is able to determine the refractive index variation of the material. Taking into account the fabrication limit, the slot width is chosen to be 30 nm in the device realization. With the other parameters $l = 800$ nm, $h = 20$ nm, the sensor theoretically shows a sensitivity of around 750 nm/RIU. Figure 4(a) gives transmission spectra for air, water ($\varepsilon_{H_2O} = 1.7161$), and ethanol ($\varepsilon_{C_2H_5OH} = 1.8322$) as analytes. Figure 4(b) shows the dip position when the refractive index of the analyte varies. The linear relation over a large refractive index range makes the device a sensor for a potentially wide domain of the analyte. Nevertheless, one can remark that the shape of the dip
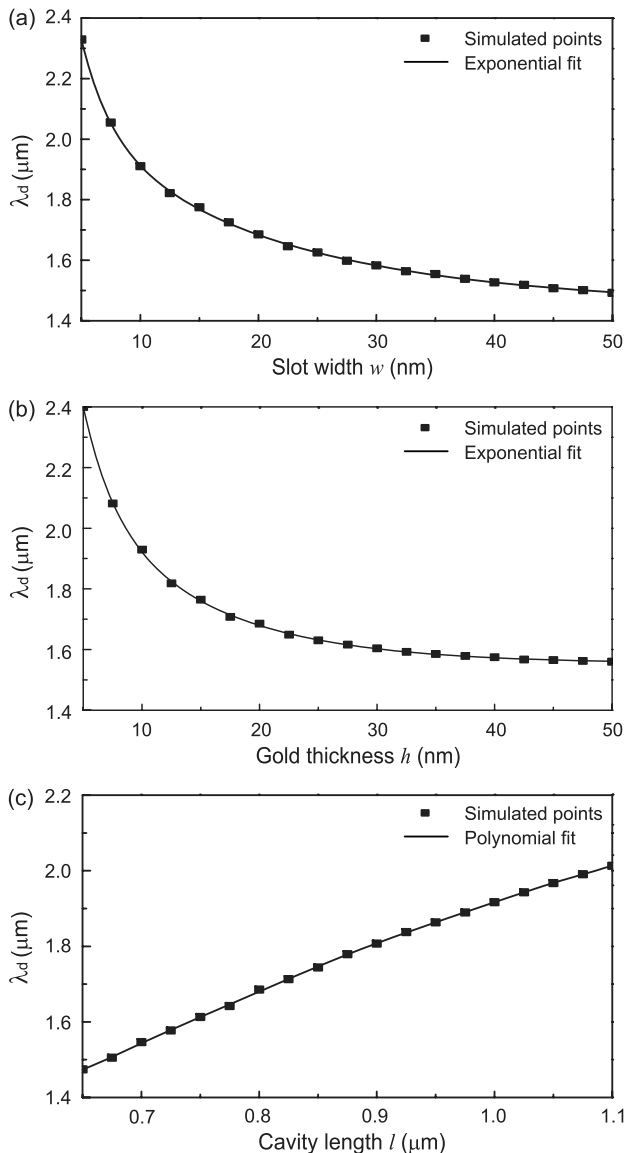
Fig. 3. Resonance position λ_d variation with geometric parameters of the cavity: (a) slot width w, (b) Au thickness h, (c) cavity length l, respectively. The basic parameters are $p = 500\,\text{nm}$, $l = 800\,\text{nm}$, $h = 20\,\text{nm}$, and $w = 20\,\text{nm}$.

evolves with the wavelength, which will be taken into account during the measurements.

3. FABRICATION

Amorphous Si (220 nm) and SiO_2 (100 nm) layers are, respectively, deposited by means of low temperature low-pressure chemical vapor deposition [17] and room temperature sputtering on a wet oxidized SiO_2 substrate ($3\,\mu\text{m}$). The cavity is fabricated by using standard e-beam lithography followed by a lift-off method [18]. Note that ZEP520A (Nippon Zeon Co.) [19] e-beam resist is used for its high sensitivity to electron bombing and its ability to achieve a high resolution and a high aspect ratio. Au (20 nm) is deposited on a Ti (1 nm) adhesion layer by e-beam evaporation. Waveguides ($15\,\mu\text{m}$ width) are created at the end of the process by reactive ion etching. Figure 5 shows the scanning electron microscopy (SEM) im-

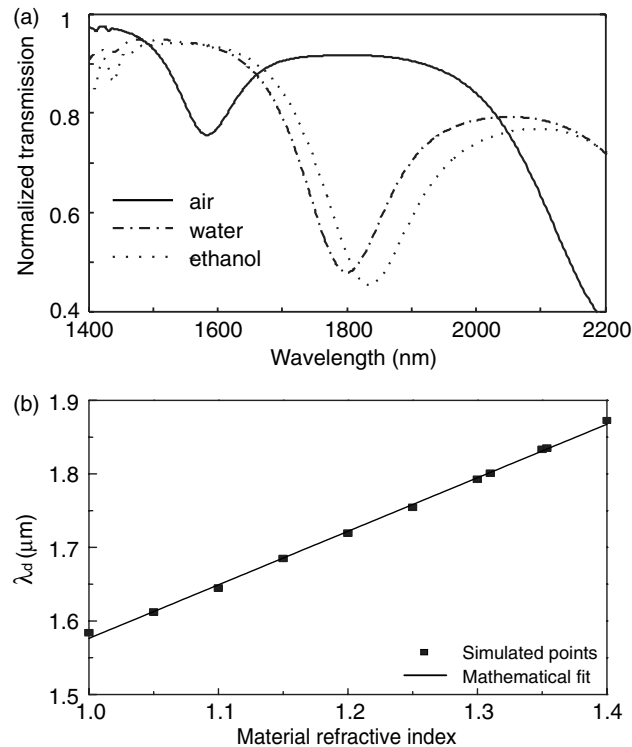Fig. 4. Optical property variation with different material refractive index filling in the $30\,\text{nm} \times 20\,\text{nm} \times 800\,\text{nm}$ slots. (a) Transmission spectra for air, water, and ethanol filling in and around the slots and (b) linear relation between the material index and the resonance position λ_d.

age of the cavity (a scheme of the full device is in the inset of Fig. 5). Note that the fabricated structure counts only 30 slots instead of an infinity in the simulated one. Nevertheless, because the structure is on top of a waveguide, which confines light transversely, we can admit that the structure is infinite. Moreover, additional calculations, not shown here, have proven that for a slot number higher than 8, a difference of only 2% is observable on the transmission spectra compared to the ideal case of the infinite structure.
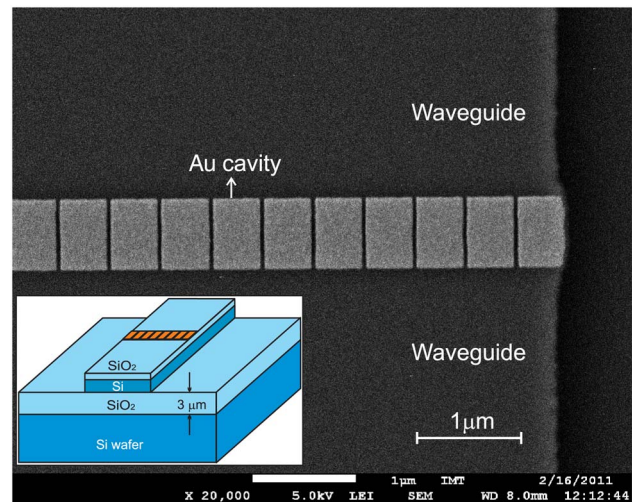

Fig. 5. (Color online) Top view of the Au cavity by SEM. Inset, scheme of the fabricated device.
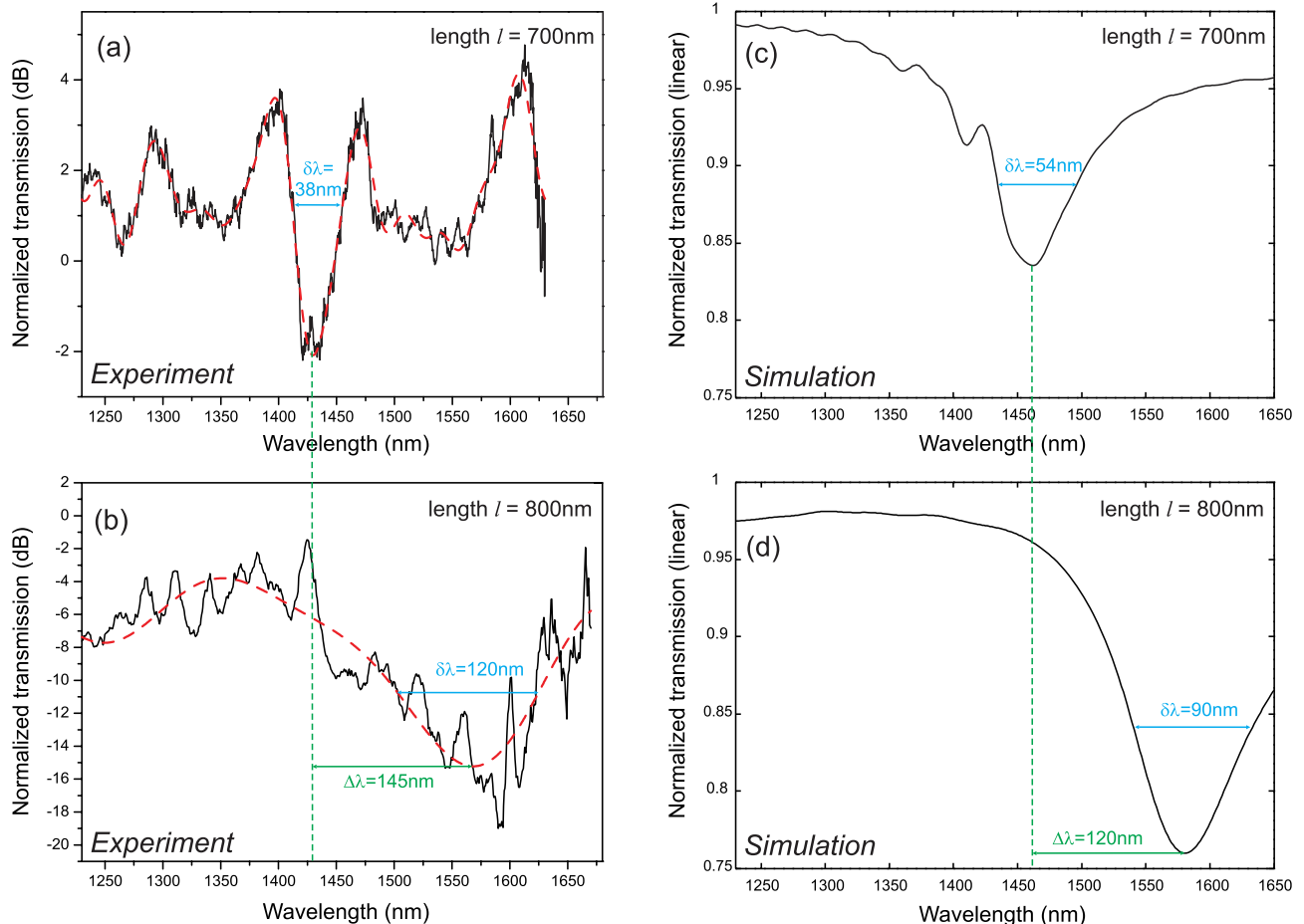
Fig. 6.   (Color online) (a), (b) Experimental results for different cavity lengths [$l = 700$ nm for (a), (c) and $l = 800$ nm for (b), (d)] in comparison with (c), (d) simulation spectra.

4. CHARACTERIZATION

Light coming from a supercontinuum (SC) white light source (Koheras, SuperK EXTREME) is coupled to the waveguide thanks to a cleaved monomode optical fiber of 1550 nm (SMF-28). The output signal is collected by another cleaved fiber connected to an optical spectrum analyzer (OSA) (Ando AQ-6315B). The combination of the OSA and the SC allows us to obtain the whole spectrum (from $\lambda = 1200$ nm to $\lambda = 1650$ nm) in one single measurement. The device has been designed in order to alternate waveguides with and without nanostructures. Therefore, a normalization of the cavity spectrum can be performed. The experimental transmission spectra are shown in Fig. 6 in comparison with the simulation results. Each experimental result (black solid curve) is fast Fourier transform filtered (red dashed curve) to get rid of parasitic oscillations. Two different cavities have been fabricated, with different lengths: $l = 700$ nm and $l = 800$ nm. One can first remark the presence of the dip in the experimental transmission spectra, which confirms the theoretical predictions: the experimental and calculated full width at half maximum ($\delta\lambda$) of the dips matches and the dip shifts $\Delta\lambda$ due to the length variation are in the same order of magnitude. The dip positions for both $l = 700$ nm and $l = 800$ nm match with the theory, although with certain deviations. Figure 3 proves that a very small variation of the geometric parameters

may generate a huge modification of the dip position λ_d, especially for the slot dimensions. In our case, a variation of 1 nm in w causes a dip shift of 8 nm and a variation of 1 nm in the Au thickness h moves the dip by 10 nm. The process of fabrication allows the utmost resolution of 2 nm in w and h. Taking all the information into account, the theoretical spectra have been verified experimentally.

5. CONCLUSION

In this paper we have shown the potential application of a metallic slot array on a dielectric waveguide to liquid or gas sensing. A theoretical sensitivity of 750 nm/RIU can be achieved on a wide refractive index range. This allows the device to be usable for a large panel of analytes (biosensing, environmental sensing). The behavior of the structure when varying the geometric parameters has been theoretically studied using 3D FDTD simulations. Moreover, the challenging steps of the fabrication process have been discussed. Coupling in the cavity by means of evanescent waves has been experimentally demonstrated to have good agreement with the theory.

ACKNOWLEDGMENTS

REFERENCES

1. X. D. Fan, I. M. White, S. I. Shopova, H. Y. Zhu, J. D. Suter, and Y. Z. Sun, "Sensitive optical biosensors for unlabeled targets: a review," Anal. Chim. Acta **620**, 8–26 (2008).
2. V. Bhatia and A. M. Vengsarkar, "Optical fiber long-period grating sensors," Opt. Lett. **21**, 692–694 (1996).
3. W. Liang, Y. Y. Huang, Y. Xu, R. K. Lee, and A. Yariv, "Highly sensitive fiber Bragg grating refractive index sensors," Appl. Phys. Lett. **86**, 151122 (2005).
4. A. Iadicicco, S. Campopiano, A. Cutolo, M. Giordano, and A. Cusano, "Refractive index sensor based on microstructured fiber Bragg grating," IEEE Photon. Technol. Lett. **17**, 1250–1252 (2005).
5. J. Homola, S. S. Yee, and G. Gauglitz, "Surface plasmon resonance sensors: review," Sens. Actuators B **54**, 3–15 (1999).
6. J. Homola, "Present and future of surface plasmon resonance biosensors," Anal. Bioanal. Chem. **377**, 528–539 (2003).
7. J. Dostalek, J. Homola, and M. Miler, "Rich information format surface plasmon resonance biosensor based on array of diffraction gratings," Sens. Actuators B **107**, 154–161 (2005).
8. S. Herminjard, L. Sirigu, H. P. Herzig, E. Studemann, A. Crottini, J. P. Pellaux, T. Gresch, M. Fischer, and J. Faist, "Surface plasmon resonance sensor showing enhanced sensitivity for CO_2 detection in the mid-infrared range," Opt. Express **17**, 293–303 (2009).
9. R. Slavik and J. Homola, "Ultrahigh resolution long range surface plasmon-based sensor," Sens. Actuators B **123**, 10–12 (2007).
10. E. Chow, A. Grot, L. W. Mirkarimi, M. Sigalas, and G. Girolami, "Ultracompact biochemical sensor built with two-dimensional photonic crystal microcavity," Opt. Lett. **29**, 1093–1095 (2004).
11. M. E. Stewart, C. R. Anderton, L. B. Thompson, J. Maria, S. K. Gray, J. A. Rogers, and R. G. Nuzzo, "Nanostructured plasmonic sensors," Chem. Rev. **108**, 494–521 (2008).
12. K. A. Willets and R. P. Van Duyne, "Localized surface plasmon resonance spectroscopy and sensing," Annu. Rev. Phys. Chem. **58**, 267–297 (2007).
13. A. G. Brolo, R. Gordon, B. Leathem, and K. L. Kavanagh, "Surface plasmon sensor based on the enhanced light transmission through arrays of nanoholes in gold films," Langmuir **20**, 4813–4815 (2004).
14. G. Veronis and S. H. Fan, "Guided subwavelength plasmonic mode supported by a slot in a thin metal film," Opt. Lett. **30**, 3359–3361 (2005).
15. J. A. Dionne, L. A. Sweatlock, H. A. Atwater, and A. Polman, "Plasmon slot waveguides: towards chip-scale propagation with subwavelength-scale localization," Phys. Rev. B **73**, 035407 (2006).
16. L. Chen, J. Shakya, and M. Lipson, "Subwavelength confinement in an integrated metal slot waveguide on silicon," Opt. Lett. **31**, 2133–2135 (2006).
17. A. Pleschinger, J. Lutz, F. Kuchar, H. Noll, and M. Pippan, "Study of polycrystalline and amorphous LPCVD silicon films by atomic force microscopy," Surf. Interface Anal. **25**, 529–532 (1997).
18. A. Perentes, I. Utke, B. Dwir, M. Leutenegger, T. Lasser, P. Hoffmann, F. Baida, M. P. Bernal, M. Roussey, J. Salvi, and D. Van Labeke, "Fabrication of arrays of sub-wavelength nano-apertures in an optically thick gold layer on glass slides for optical studies," Nanotechnology **16**, S273–S277 (2005).
19. K. Kurihara, K. Iwadate, H. Namatsu, M. Nagase, H. Takenaka, and K. Murase, "An electron beam nanolithography system and its application to Si nanofabrication," Jpn. J. Appl. Phys. **34**, 6940–6946 (1995).